

1 **Parametrizations of size distribution and refractive index of biomass burning**
2 **organic aerosol with black carbon content**

3 **Biao Luo^{1,2}, Ye Kuang^{1,2,*}, Shan Huang^{1,2*}, Qicong Song^{1,2}, Weiwei Hu³, Wei Li^{1,2}, Yuwen Peng^{1,2},**
4 **Duohong Chen⁴, Dingli Yue⁴, Bin Yuan^{1,2}, Min Shao^{1,2}**

5 ¹ Institute for Environmental and Climate Research, Jinan University, Guangzhou, China.

6 ² Guangdong-Hongkong-Macau Joint Laboratory of Collaborative Innovation for Environmental
7 Quality, Guangzhou, China.

8 ³ State Key Laboratory of Organic Geochemistry and Guangdong Key Laboratory of Environmental
9 Protection and Resources Utilization, Guangzhou Institute of Geochemistry, Chinese Academy of
10 Sciences, Guangzhou 510640, China

11 ⁴ Guangdong Ecological and Environmental Monitoring Center, State Environmental Protection Key
12 Laboratory of Regional Air Quality Monitoring, Guangzhou 510308, China

13 Corresponding author: Ye Kuang (kuangye@jnu.edu.cn) and Shan Huang

14 (shanhuang_ece@jnu.edu.cn)

15
16
17
18
19
20
21
22
23
24
25
26

27	Table of contents	
28	1. Methods.....	3
29	1.1 The modelling method of <i>AAEBC</i> , $\lambda - 880$	3
30	Figure S1. (a) Average size distributions of AS and AN under different NR_PM1 conditions, dashed lines	
31	are lognormal fitting curves; (b) Simulated PM1 MSE of AS and AN under different NR_PM1 conditions	
32	and corrected ones	4
33	1.2 Mass Scattering Efficiency calculations for different aerosol components.	4
34	Figure S2. (a) Average OA size distributions, and parts associated with HOA and BBOA, D_{va} is the vacuum	
35	aerodynamic diameter. (b) The average OA size distributions with contributions of HOA and BBOA	
36	subtracted, and the remaining can be well fitted using two lognormal modes.....	5
37	1.3 Refractive index retrieval	6
38	2. Other figures	8
39	Figure S3. (a) Mass spectral profile in family groups and (b) time series of PMF OA components. Also	
40	exhibited are concentration variations of tracer compounds on the right axes.	8
41	Figure S4. Normalized average Cx distribution measured by the SP-AMS.	9
42	Figure S5. Photoed at at the Heshan supersite during the observation period.	10
43	Figure S6. (a) Diurnal variations of BBOA and HOA; (b) The distribution of BBOA/HOA ratio.....	11
44	Figure S7. (a) to (c) Time series of resolved OA factors by SP-AMS measurements, and (d) is the derived BrC	
45	absorption coefficients at 370 nm. Shaded areas represent identified spikes.	12
46	Figure S8. Examples of identifying differences of PNSD (Δ PNSD) and PVSD (Δ PVSD).....	13
47	Figure S9. Average OA size distribution differences for spikes in Fig.3b, and the difference can be fitted	
48	using two lognormal modes, corresponding to HOA and BBOA respectively.	14
49	Figure S10. Variations of BBOA MSE under different Dgv, Dgn and σ_g conditions.....	15
50	References.....	16
51		
52		
53		
54		
55		
56		
57		
58		
59		
60		
61		
62		

63
64
65

66 1. Methods

67 1.1 The modelling method of $AAE_{BC,\lambda}$ -880

68 The absorption coefficient $\sigma_{abs,Mie,\lambda}$ was obtained by the following:

$$69 \sigma_{abs,Mie,\lambda} = \int Q_{abs,Mie,\lambda}(Dp) * \left(\frac{\pi}{4} D_p^2\right) N(\log D_p) * d_{\log D_p} \quad (1)$$

70 where $N(\log D_p)$ is the PNSD function, $Q_{abs,Mie,\lambda}$ is absorption efficiency which is simulated using
71 the Mie-theory, D_p is the particle. For D_p bin, particles are classified into three types: non-light-
72 absorbing particles (Non-BC), BC-containing particles and pure BC particles. Parameters r_{ext} defined
73 as mass fraction of pure externally mixed BC (M_{ext}) to total BC mass (M_{BC}) in different diameter bins
74 and R_NBC defined as the number fraction of particles that does not contain BC are used to represent
75 BC mixing state. The PNSD of Non-BC particles ($N(\log D_p)_{Non-BC}$) and BC-containing particles
76 ($N(\log D_p)_{BC}$) can be given by the following equations:

$$77 N(\log D_p)_{Non-BC} = N(\log D_p)_{measure} * R_NBC \quad (2)$$

$$78 N(\log D_p)_{BC} = N(\log D_p)_{measure} * (1 - R_NBC) \quad (3)$$

79 $N(\log D_p)_{measure}$ is the PNSD measured by the SMPS and APS. The PNSD of pure BC particles
80 ($N(\log D_p)_{ext}$) and core-shell mixed BC particles ($N(\log D_p)_{core-shell}$) can be given by the
81 following equations:

$$82 r_{ext} = \frac{M_{ext}}{M_{BC}} \quad (4)$$

$$83 N(\log D_p)_{ext} = N(\log D_p)_{BC} * f_{ext}(Dp) \quad (5)$$

$$84 N(\log D_p)_{core-shell} = N(\log D_p)_{BC} * (1 - f_{ext}(Dp)) \quad (6)$$

85 $f_{ext}(Dp)$ is volume fraction of pure BC at each diameter bin which can be calculated by :

$$86 f_{ext}(Dp) = \frac{M_{BC}(Dp) * r_{ext}}{\rho_{BC} * N(\log D_p)_{BC} * \left(\frac{\pi}{6} D_p^3\right)} \quad (7)$$

87 where ρ_{BC} is the density of BC (1.5 g cm^{-3}); M_{BC} is derived from AE33. Size distribution of BC
88 mass $M_{BC}(Dp)$ is calculated based on the normalized Cx fraction $f_{Cx}(Dp)$ at each diameter bin:

$$89 M_{BC}(Dp) = M_{BC} \times f_{Cx}(Dp) \quad (8)$$

90 In addition to the PNSD of the three types of particles mentioned above, another key parameter of

91 the core-shell model is the diameter of the BC core, at each diameter bin the D_{core} is calculated as:

$$92 \quad D_{core} = \left(\frac{6 \times M_{BC}(Dp) \times (1 - r_{ext})}{\rho_{BC} \times \pi} \right)^{1/3} \quad (9)$$

93 After obtaining the absorption coefficient at each wavelength, the AAE at two wavelengths is
 94 calculated as the following equation:

$$95 \quad AAE_{\lambda_1 - \lambda_2} = \frac{\ln(\sigma_{abs, \lambda_1}) - \ln(\sigma_{abs, \lambda_2})}{\ln(\lambda_1) - \ln(\lambda_2)} \quad (10)$$

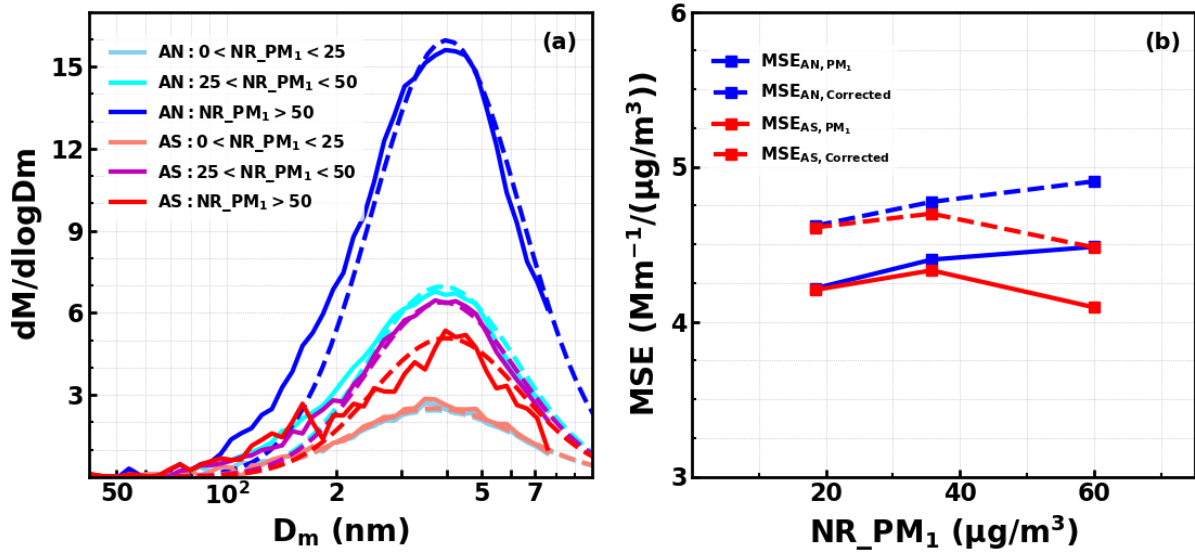


Figure S1. (a) Average size distributions of AS and AN under different NR_PM1 conditions, dashed lines are lognormal fitting curves; (b) Simulated PM1 MSE of AS and AN under different NR_PM1 conditions and corrected ones

96
 97

98 1.2 Mass Scattering Efficiency calculations for different aerosol components.

99 The size distributions of ammonium (AN) nitrate and ammonium sulfate (AS) paired from measured size
 100 distributions of nitrate, ammonium and sulfate by the SP-AMS under different non-refractory mass concentrations of
 101 PM1 (NR_PM1, PM1 corresponds to aerosols with aerodynamic diameter less than 1 μm) is shown in Fig.S1a. Note
 102 that the D_m converted by assuming an aerosol density of 1.6 g/cm^3 from the SP-AMS vacuum aerodynamic diameter
 103 D_{va} . The $MSE_{AN, PM1}$ defined as $MSE_{PM1} = \frac{\sigma_{sp, PM1}}{AN_{PM1}}$ under different NR_PM1 conditions and results of $MSE_{AS, PM1}$
 104 are shown in Fig.S1b. The density of AS and AN are 1.769 and 1.72 g/cm^3 , and used refractive index of AS and AN
 105 is $1.53 \cdot 10^{-7}i$. However, in this study, the aerosol scattering coefficient of PM10 (aerosols with aerodynamic diameter

106 less than 10 μm) and the aerosol mass concentration of PM_{10} is measured by the SP-AMS. Therefore, the corrected
 107 MSE defined as $MSE_{Corrected} = \frac{\sigma_{sp,PM10}}{AN_{PM1}} = MSE_{PM1} \times C$ is simulated and also shown in Fig.1b, and C is the
 108 correction factor. The average $MSE_{Corrected}$ values for AS and AN are 4.6 and 4.8 m^2/g , and used in this study.
 109 The MSE_{HOA} is simulated on the basis of identified average HOA D_{gv} and σ_g of 180 nm and 1.46 using the Mie
 110 theory in combination with calculated HOA density of 1.15 g/cm^3 . The calculated MSE_{HOA} is 3.2 m^2/g .
 111 The MSE_{BC} is simulated using the normalized Cx distribution shape shown in Fig.s4, and assuming an BC density
 112 of 1.5 g/cm^3 and BC refractive index of 1.8-0.54i. The calculated MSE_{BC} is 2.8 m^2/g .
 113 The average size distributions of OA measured by the SP-AMS during the entire campaign is shown in Fig.S2a. The
 114 average size distributions of HOA and BBOA calculated from average HOA and BBOA mass concentrations together
 115 with identified average D_{gv} and σ_g of HOA and BBOA identified from SP-AMS measurements (175, 395 and 1.46,

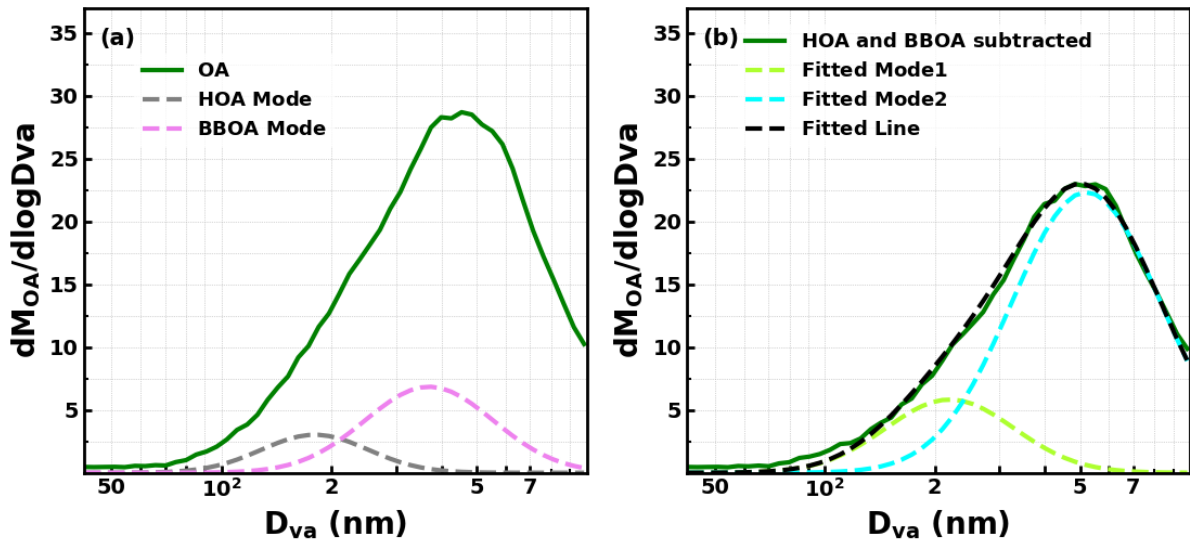


Figure S2. (a) Average OA size distributions, and parts associated with HOA and BBOA, D_{va} is the vacuum aerodynamic diameter. (b) The average OA size distributions with contributions of HOA and BBOA subtracted, and the remaining can be well fitted using two lognormal modes.

116 1.55 for HOA and BBOA as shown in Fig.Sx) are also shown in Fig.S2a. If the contributions of HOA and
 117 BBOA are subtracted (Fig.S2b), the OA size distribution can be well fitted using two lognormal modes. The mass
 118 concentration of fitted Mode 1 is consistent that of aBBOA and obviously different with mass concentrations of other
 119 remaining OA factors, and mass concentration of fitted Mode 2 is consistent with the sum of LOOA, MOOA and
 120 Night-OA. Thus, the Mode 1 is identified as the size distribution of aBBOA. The Mode 2 of LOOA, MOOA and
 121 Night-OA suggests that most secondary organic aerosols during this campaign are likely internally mixed. Thus the

122 MSE_{aBBOA} is simulated as 4.5 m²/g with identified size distribution of Mode 1 and calculated aBBOA
 123 density g/cm³ using the scheme proposed by ³. Corrected MSE of MOOA, Night-OA, LOOA (MSE_{SOA})
 124 is calculated as 6.3 m²/g with identified size distribution of Mode 2 and estimated average density of
 125 1.31 g/cm³ using volume weighting rule.

126 1.3 Refractive index retrieval

127 Determined BBOA MSEs and MAEs were converted to Volume scattering or absorption
 128 efficiency (VSE or VAE) through VSE=MSE*density. With given geometric mean (D_{gn}) and standard
 129 deviation (σ_g) values of the PNSD. The assuming total number concentration of 1000 (N_{tot}=1000
 130 /cm³), PNSD can be given as :

$$131 \quad N(\log D_p) = \frac{dN}{d\log D_p}(D_p) = \frac{N_{tot}}{\sqrt{2\pi} \log(\sigma_g)} \exp \left[-\frac{(\log(D_p) - \log(D_{gn}))^2}{2 \log^2 \sigma_g} \right] \quad (11)$$

132 The with given refractive index of $m = m_{R,BBOA} + m_{i,BBOA} \times i$, the aerosol scattering efficiency Q_{sca} and
 133 absorption efficiency Q_{abs} can be calculated using the Mie theory. And then scattering and absorption
 134 coefficients of bulk aerosols can be derived as:

$$135 \quad \sigma_{sca}(\lambda) = \int_0^{D_p^{max}} Q_{sca}(m, \lambda, D_p) \times \frac{\pi}{4} D_p^2 \times N(\log D_p) \times d\log D_p \quad (12)$$

$$136 \quad \sigma_{abs}(\lambda) = \int_0^{D_p^{max}} Q_{abs}(m, \lambda, D_p) \times \frac{\pi}{4} D_p^2 \times N(\log D_p) \times d\log D_p \quad (13)$$

137 Where λ is the optical wavelength, and D_p^{max} of 2500 nm is set. The total volume concentration can be
 138 calculated as:

$$139 \quad V_{tot} = \int_0^{D_p^{max}} \frac{\pi}{6} D_p^3 \times N(\log D_p) \times d\log D_p \quad (14)$$

140 Then the VSE and MAE can be calculated as:

$$141 \quad VSE(\lambda) = \frac{\sigma_{sca}(\lambda)}{V_{tot}} \quad (15)$$

$$142 \quad VAE(\lambda) = \frac{\sigma_{abs}(\lambda)}{V_{tot}} \quad (16)$$

143 The $m_{R,BBOA}$ was retrieved through varying $m_{R,BBOA}$ in iterations to find a $m_{R,BBOA}$ with which the derived
 144 VSE can be reproduced, in these iterations $m_{i,BBOA}$ was parameterized with the corresponding
 145 $\Delta CO / \Delta BBOA$ using the relationships determined in Sect.3.4. The $m_{i,BBOA}$ was retrieved through varying
 146 $m_{i,BBOA}$ in iterations to find a $m_{R,BBOA}$ with which the derived VAE can be reproduced, and $m_{R,BBOA}$ are
 147 fixed as 1.6 due to that sensitivity tests show that very small influences of $m_{R,BBOA}$ variations on $m_{i,BBOA}$

148 retrieval.

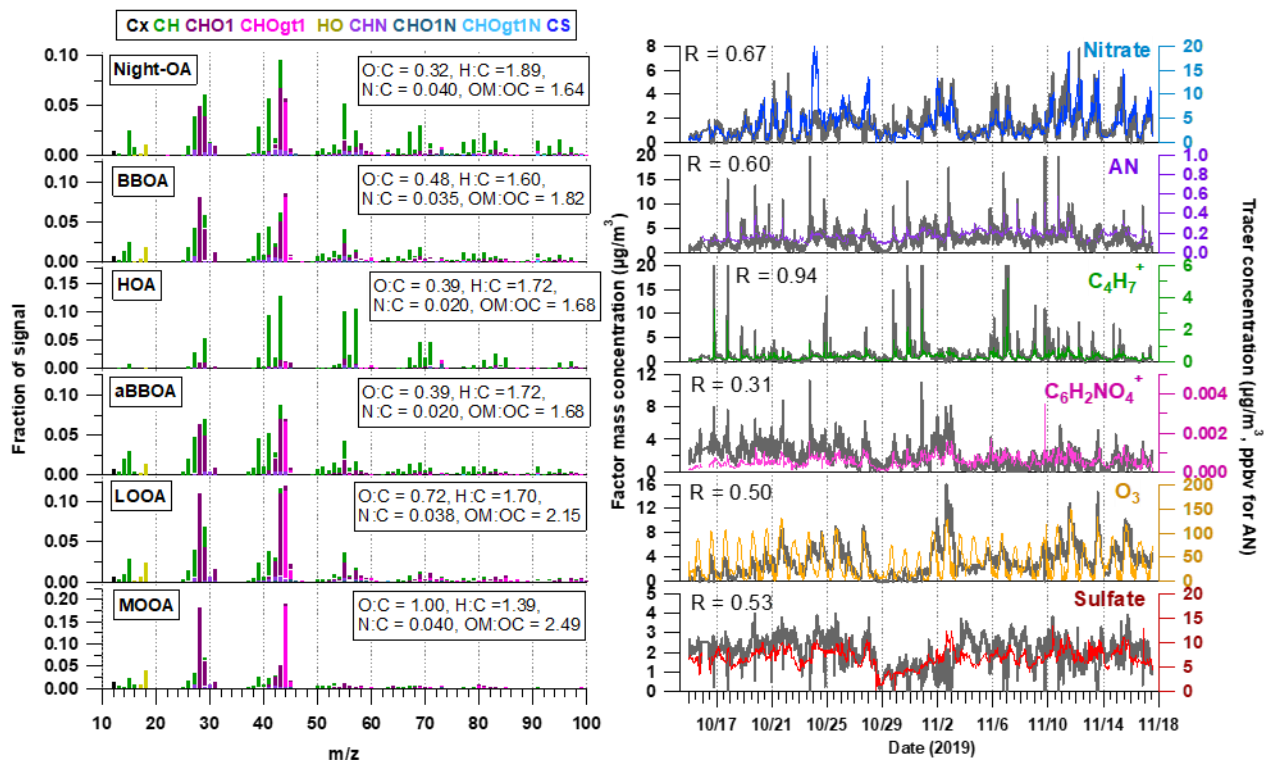
149

150

151

152 **2. Other figures**

153
154
155

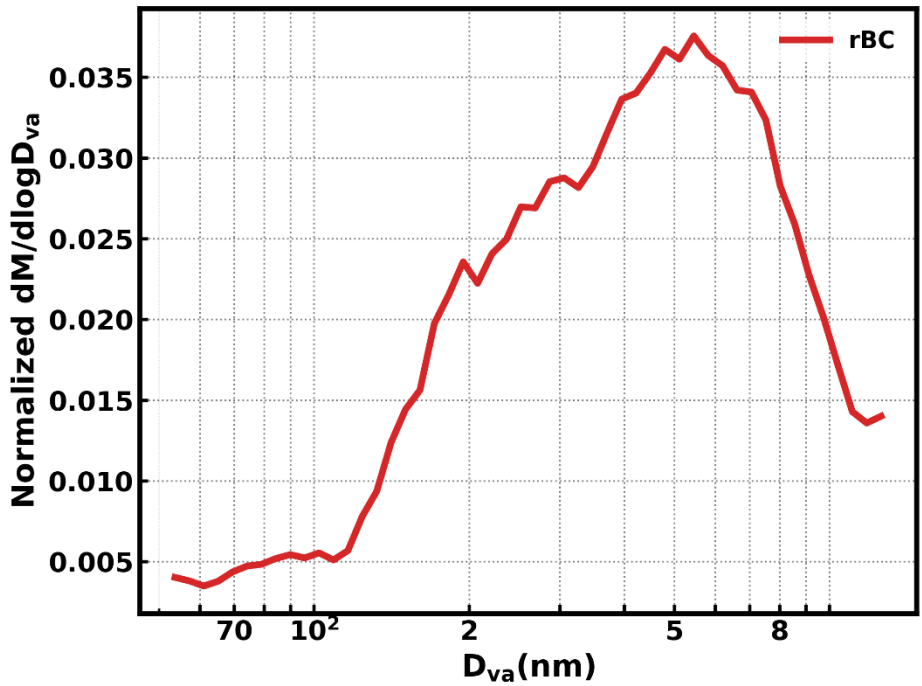


156

157 **Figure S3. (a)** Mass spectral profile in family groups and **(b)** time series of PMF OA components. Also exhibited are
158 concentration variations of tracer compounds on the right axes.

159
160
161
162
163
164
165
166
167
168
169
170
171
172
173
174
175

176
177

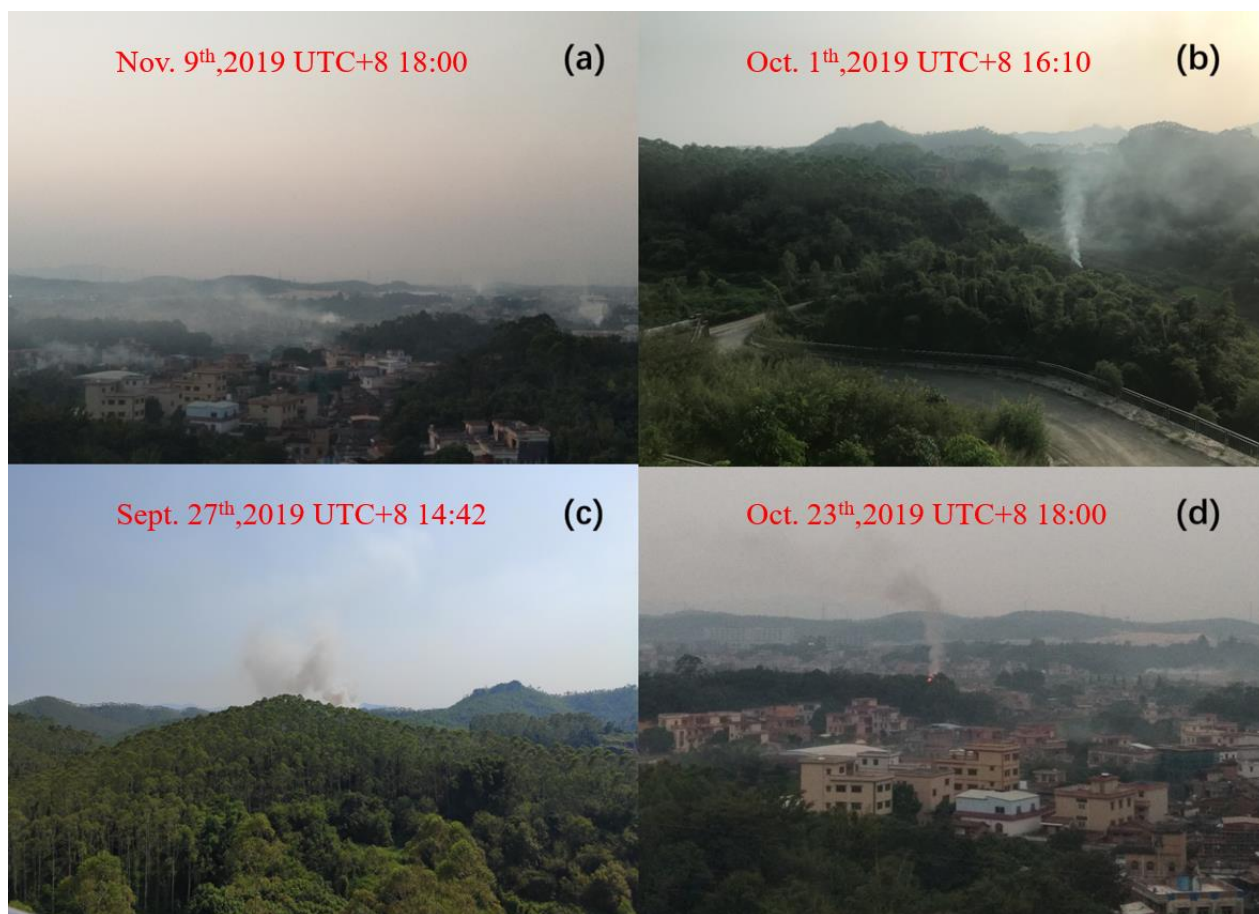


178

179 Figure S4. Normalized average Cx distribution measured by the SP-AMS.

180
181
182
183
184
185
186
187
188
189
190
191
192
193
194
195
196
197
198
199
200

201
202
203
204

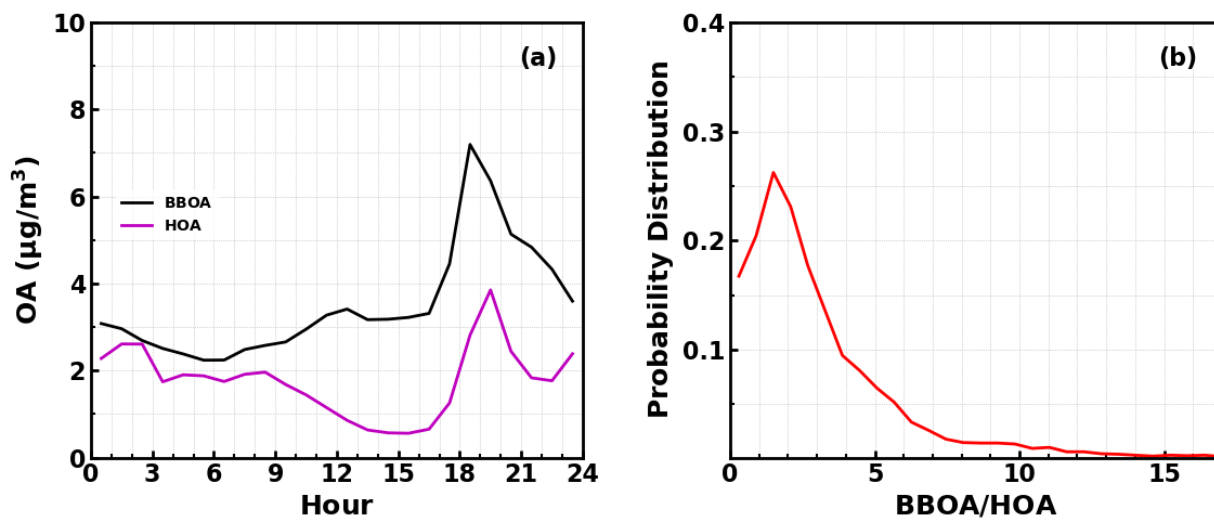


205

206 **Figure S5.** Photoed at at the Heshan supersite during the observation period.

207
208
209
210
211
212
213
214
215
216
217
218
219
220
221

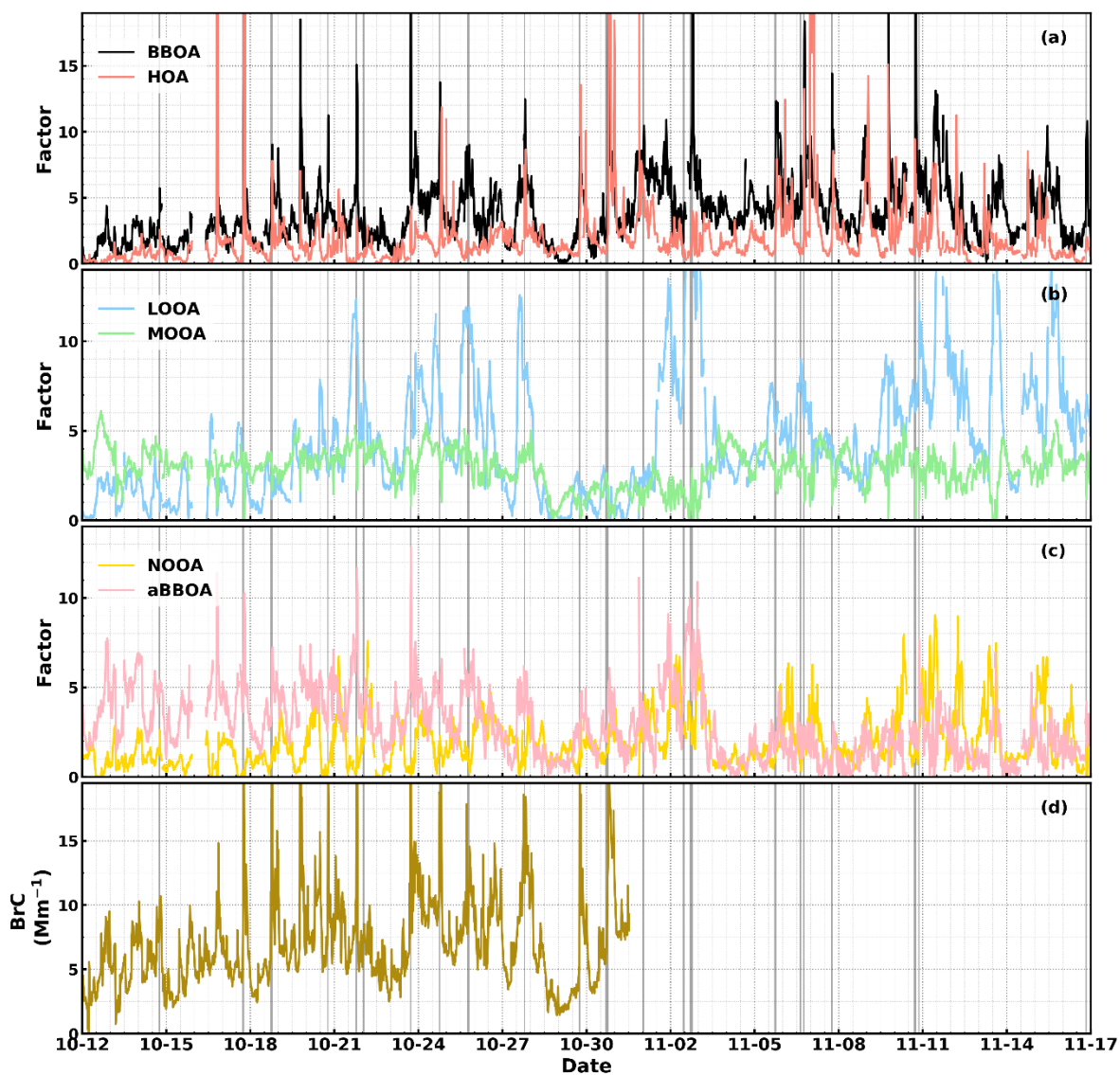
222
223
224
225
226



227

228 Figure S6. (a) Diurnal variations of BBOA and HOA; (b) The distribution of BBOA/HOA ratio.

229



230

231 **Figure S7. (a) to (c)** Time series of resolved OA factors by SP-AMS measurements, and **(d)** is the derived BrC absorption
 232 coefficients at 370 nm. Shaded areas represent identified spikes.

233

234

235

236

237

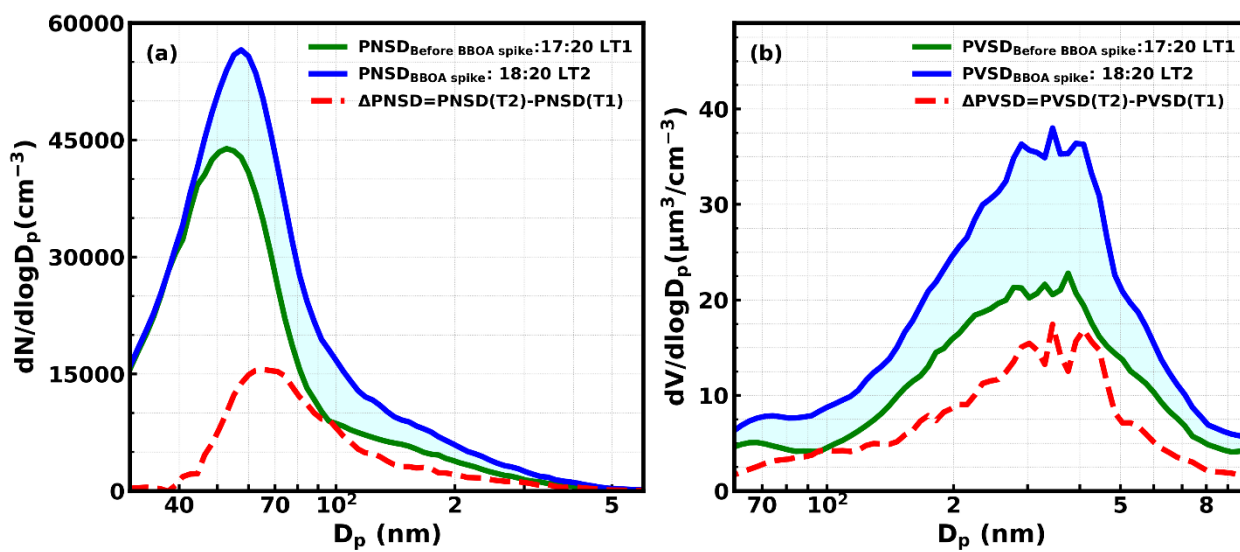
238

239

240

241

242
243
244
245
246
247
248
249
250
251



252

253 **Figure S8.** Examples of identifying differences of PNSD (ΔPNSD) and PVSD (ΔPVSD)

254
255
256
257
258
259
260
261
262
263
264
265
266
267
268
269

270
271
272
273
274
275
276
277
278
279
280
281
282
283
284
285
286
287

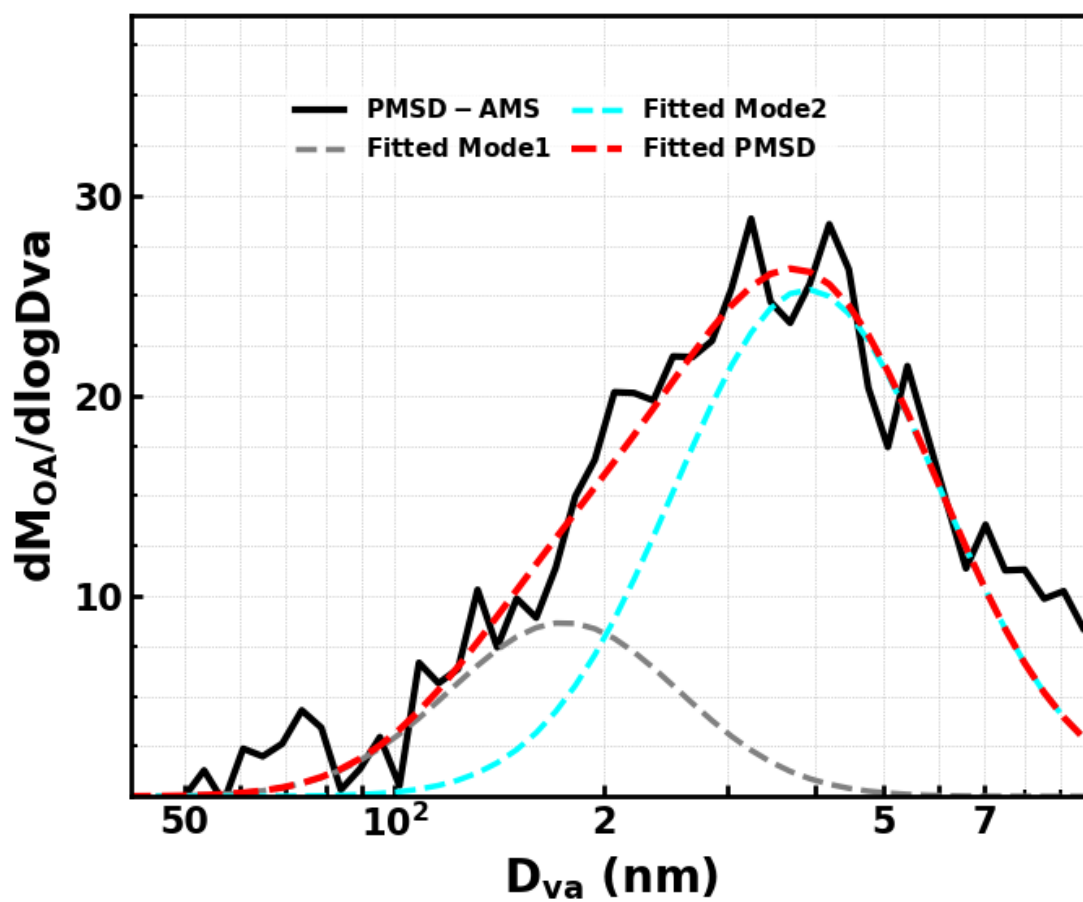


Figure S9. Average OA size distribution differences for spikes in Fig.3b, and the difference can be fitted using two lognormal modes, corresponding to HOA and BBOA respectively.

288
289
290
291
292
293
294
295
296

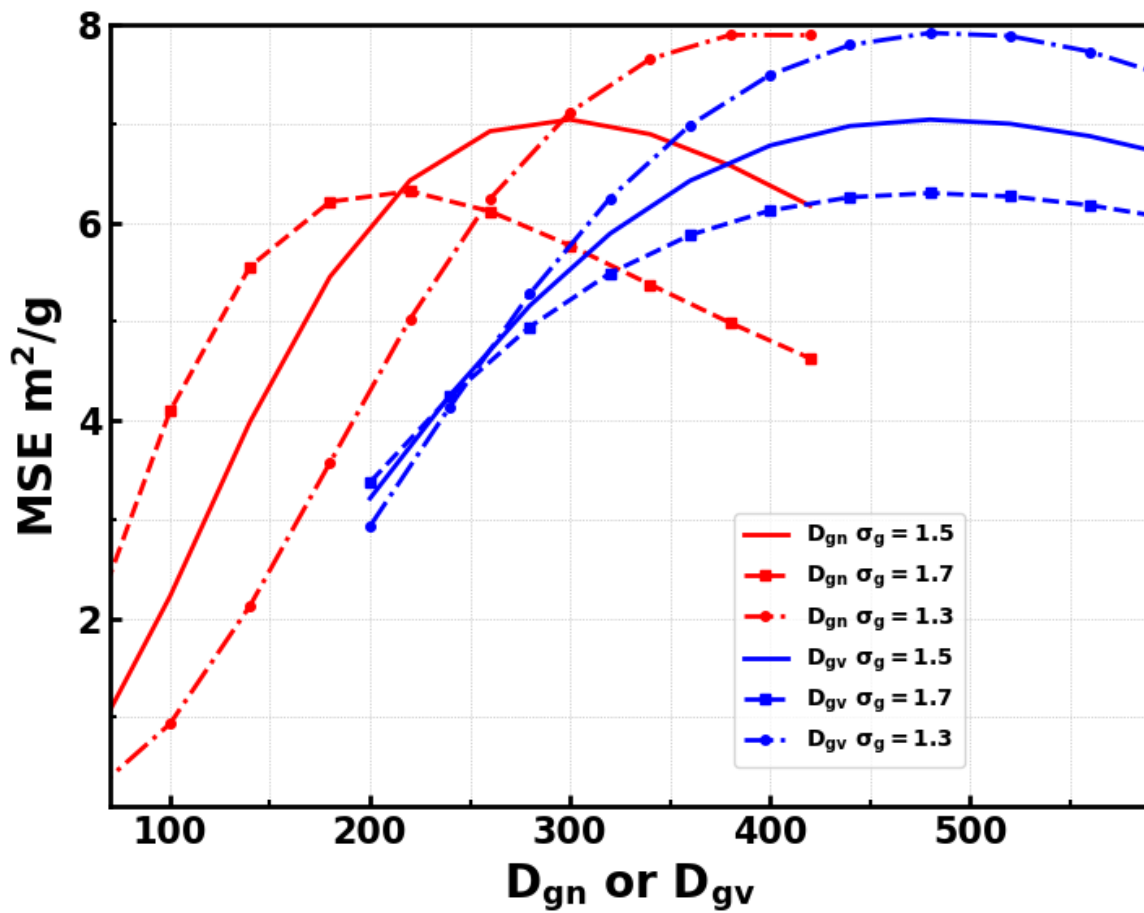


Figure S10. Variations of BBOA MSE under different D_{gv} , D_{gn} and σ_g conditions.

297
298
299
300
301
302
303
304
305

306

307

308 **References**

309 (1). Yi Ming Qin^{1, a, b}, Hao Bo Tan², Yong Jie Li³, Zhu Jie Li^{2,4}, Misha I. Schurman^{5,c}, Li Liu^{2,6}, Cheng Wu⁷, and Chak K.
310 Chan^{1,b,c}, Chemical characteristics of brown carbon in atmospheric particles at a suburban site near Guangzhou, China.

311 **2018.**

312 (2). Ma, N.; Zhao, C. S.; Müller, T.; Cheng, Y. F.; Liu, P. F.; Deng, Z. Z.; Xu, W. Y.; Ran, L.; Nekat, B.; van Pinxteren, D.; Gnauk,
313 T.; Müller, K.; Herrmann, H.; Yan, P.; Zhou, X. J.; Wiedensohler, A., A new method to determine the mixing state of light
314 absorbing carbonaceous using the measured aerosol optical properties and number size distributions. *Atmos. Chem. Phys.*

315 **2012**, 12, (5), 2381-2397.

316 (3). Kuwata, M.; Zorn, S. R.; Martin, S. T., Using Elemental Ratios to Predict the Density of Organic Material Composed of
317 Carbon, Hydrogen, and Oxygen. *Environmental science & technology* **2012**, 46, (2), 787-794.

318